Railway Sciences

The impact of metal cleaning agents on components of air conditioning piping systems in EMUs

Wei Du
Metals and Chemistry Research Institute, fem Research Institute for Precious Metals and Metal Chemistry, Beijing, China
Bingzu Li
China Railway Lanzhou Bureau Group Co., Ltd, Research and Technology Supervision Institute, Lanzhou, China
Yanpin Zhu
China Railway Wuhan Bureau Group Co., Ltd., Scientific and Technological Research Institute, Wuhan, China
Lunan Jia
Qingdao EMU Depot, China Railway Jinan Bureau Group Co., Ltd, Qingdao, China
Dehong Zhang
Guangzhou EMU Depot, China Railway Guangzhou Group Co., Ltd, Guangzhou, China
Zhongyu Yi
Metals and Chemistry Research Institute, fem Research Institute for Precious Metals and Metal Chemistry, Beijing, China, and
Ruohan Xiang and Yishuo Liu
China Academy of Railway Sciences Corporation Limited, Metals and Chemistry Research Institute, Beijing, China

Received 24 February 2026
Revised 16 April 2026
Accepted 6 May 2026

Abstract

Purpose – In response to the problems of performance degradation, sealing failure and medium leakage of metal components in air conditioning pipelines due to material corrosion, this study intends to lay the foundation for exploring the causes of corrosion and optimising anti-corrosion measures in the future, ensuring the safe and stable operation of air conditioning pipelines.

Design/methodology/approach – Systematic investigation of corrosion mechanisms and cleaning agent effects was conducted using scanning electron microscopy (SEM), atomic force microscopy, corrosive element detection and cleaning agent immersion tests.

Findings – Findings indicate dense corrosion pitting on the tail surface of air conditioning copper tubes (TP2 deoxidised copper), with enriched corrosive Cl and P elements serving as primary corrosion drivers. Under continuous immersion, metal corrosion rates significantly exceed air exposure conditions. Both acidic and alkaline cleaning agents exhibit stronger corrosive effects on carbon steel pressure sections and copper tubes than neutral cleaning agents.

Originality/value – The main factors causing corrosion of TP2 deoxygenated copper pipes in air conditioning, the effects of different environments, and types of cleaning agents on the corrosion of pipeline metals have been

Funding: This work is supported by Metal coating anti-corrosion technology for typical components of power lines (2023YJ078)

Railway Sciences
Emerald Publishing Limited
e-ISSN: 2755-0915
p-ISSN: 2755-0907
DOI 10.1108/RS-02-2026-0010

identified in the study. It provides reliable theoretical support for the optimisation of anti-corrosion design and scientific selection of cleaning agents for air conditioning pipelines.

Keywords Metal cleaning agents, EMU, Air conditioning piping system, Corrosion

Paper type Research article

1. Introduction

As a critical component connecting the compressor to the circulation system, the air conditioning pipeline of EMUs primarily functions to absorb compressor vibrations through flexible metal hoses (such as corrugated pipes with stainless steel mesh sleeves), thereby reducing pipeline system noise and mechanical stress. However, corrosion issues primarily arise from multiple coupled factors. On one hand, environmental influences–including sand and dust impact during high-speed operation, industrial contaminants (such as oil films and particulates), and temperature-humidity cycling–can compromise the pipeline surface protective layer, accelerating electrochemical corrosion (Liu, Xu, Chen, & Zhang, 2026). For instance, condensation accumulation beneath insulation layers can induce microbiologically influenced corrosion (MIC), leading to comprehensive pipeline failure within short timeframes. Concurrently, material factors play a role: certain sealing materials exhibit inadequate temperature resistance, while ageing of air springs (e.g. photo-oxygen degradation triggered by ultraviolet radiation) diminishes vibration damping capabilities, indirectly heightening pipeline stress corrosion risks (Abd El-Maksoud, 2018; Cheng, Meng, Wang, Pang, & Duo, 2021; Tan *et al.*, 2017; Zheng, Gong, Li & Guo, 2018; Zhu *et al.*, 2025).

Corrosion-induced degradation of piping performance directly jeopardises train operational safety. It diminishes mechanical properties, reducing flexibility and pressure-bearing capacity, thereby amplifying vibration transmission. This results in increased carriage noise, diminished passenger comfort, and accelerated fatigue damage to other vehicle components. It also heightens leakage risks, as corrosion perforations may cause refrigerant (e.g. Freon) leaks, resulting in air conditioning system failure. Incidents have occurred where refrigerant leakage from vibration-damping hoses triggered cooling failures, necessitating emergency shutdowns for repairs and severely compromising operational safety.

Air conditioning unit piping, comprising copper tubing (TP2 deoxidised copper) and stainless steel corrugated hoses (304 grade), exhibits corrosion during operation, as illustrated in Figure 1. 3 levels of air conditioning pipe corrosion: Minor corrosion: Small, isolated rust spots cover no more than 10mm^2 with no larger than 16mm^2 areas, and no extensive flaking or accumulation; Moderate corrosion: Extensive, patchy, or block-like rust spots and verdigris are present, but no refrigerant leakage has occurred; Severe corrosion: Beyond moderate corrosion, rust has penetrated the pipe interior, resulting in refrigerant leakage (Bai *et al.*, 2013; Eddy, Ibok, Ebenso, El Nemr, & El Ashry, 2009; El Nemr *et al.*, 2014a, b; El Nemr, Moneer, Khaled, Khaled, & El-Said, 2014; Li, Bae, Mishrra, Shi, & Giammar, 2020; Thombare *et al.*, 2022).

2. Experiment

The corrosion test specimens of air conditioning copper tube were sourced from Changsha EMU Depot, measuring 40 × 20 mm. Section A represents the tail end of the copper tube, while Section B denotes the head end, as illustrated in Figure 2. The high-pressure shock-absorbing hose for air conditioning compressors was procured from Beijing Zhuoxu Company, measuring 50 × 2 cm, as shown in Figure 3.

2.1 Analysis of corrosion samples

A 10 × 10 mm corrosion sample was excised. The surface morphology of the corrosion rust layer was observed and analysed using a scanning electron microscope. The elemental composition of the rust layer was characterised via the instrument's integrated X-ray energy

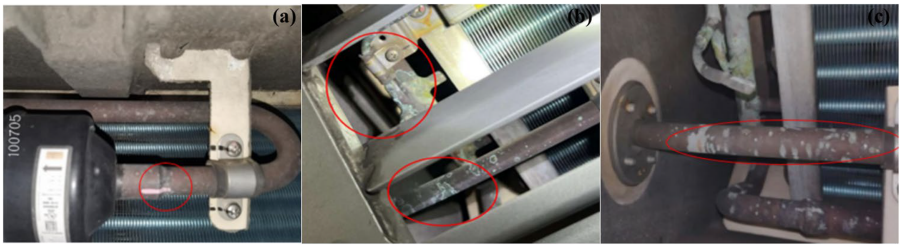

Figure 1. (a) Mild corrosion (b) Moderate corrosion (c) Severe corrosion. **Source (s):** Authors' own work

Figure 2. Corrosion sample of air conditioning copper tube. **Source (s):** Authors' own work

Figure 3. High-pressure shock absorber hose. **Source (s):** Authors' own work

dispersive spectrometer. Test equipment models: Electron microscope (TESCAN MIRA4), Energy dispersive spectrometer (Xplore 30)

A handheld portable microscope was employed to examine the macroscopic corrosion morphology at representative locations within the specimens. The microscope featured 1.3 million pixels and a resolution of 1280 × 1024 (MJPG). Instrument model: Anyth.

2.2 Effect of cleaning agents on high-pressure shock-absorbing hoses

Following GB/T1690-2010 "Test Methods for Resistance of Vulcanised Rubber or Thermoplastic Rubber to Liquids" (National Standardization Administration, 2011), the high-pressure shock-absorbing hose of an air conditioning compressor was sectioned into 3 components: corrugated hose (304 stainless steel), pressure-bearing section (carbon steel), and copper tube (TP2 deoxidised copper). Each section underwent full immersion testing in cleaning agents, as illustrated in Figure 4 and detailed in Table 1.

Contact angle measurement can reflect wettability. The smaller the contact angle, the better the wetting performance of the liquid on the solid surface. The contact angles of four cleaning agents were measured according to the method specified in GB/T 30,693–2014 "Plastics—

Figure 4. Appearance of the sample after cutting the suspension hose of the air conditioning unit. **Source (s):** Authors' own work

Table 1. Types of cleaning agents

Cleaning agent type	Undiluted pH value	Cleaning efficiency/%	Contact angle/°
Cleaning Agent 1# (Acidic)	1.7	80	32
Cleaning Agent 4# (Acidic)	0.8	69	36
Cleaning Agent 5# (Neutral)	7.2	75	33
Cleaning Agent 6# (Alkaline)	9.0	86	28

Source(s): Authors' own work

Thin Films and Sheets—Determination of Contact Angle." The cleaning performance was tested according to the method outlined in Q/CR468-2025 "Cleaning Agents for External Surfaces of Electric Multiple Units." The test results are shown in Table 1.

Experiment 1: Prepare cleaning agents 1#, 4#, 5#, and 6# at a dilution concentration of 20%. After continuous immersion of bellows, pressure-bearing sections, and copper tubes in the diluted solutions for 168 hours, observe changes in specimen appearance and corrosion quality.

Experiment 2: Prepare cleaning agents 1#, 4#, 5#, and 6# at a dilution concentration of 20%. Apply the cleaning agent solution to the surfaces of corrugated pipes, pressure-bearing sections, and copper tubes. Expose the specimens to air for 24 hours. After 7 cycles, observe changes in specimen appearance and corrosion mass.

Following the aforementioned tests, specimens underwent microphotography and SEM analysis.

AFM testing: Analysis of specimen surfaces was conducted using a Bruker Dimension Icon instrument.

3. Results and discussion

3.1 Analysis of air conditioning copper tube corrosion

3.1.1 Optical microscope observation.. The morphology of corrosion products on the copper tube within the high-pressure shock-absorbing hose of an air conditioning compressor was captured using a handheld microscope (The microscope featured 1.3 million pixels and a resolution of 1280×1024 (MJPG). As shown in Figure 5, multiple corrosion patches were observed on the surface of the copper tube's tail section, with severe blackening of the patches. No extensive corrosion was observed on the head section of the copper tube, as depicted in Figure 6 (Deyab, Mohsen & Guo, 2022; Olasunkanmi, Obot, Kabanda, & Ebenso, 2015; Liu,

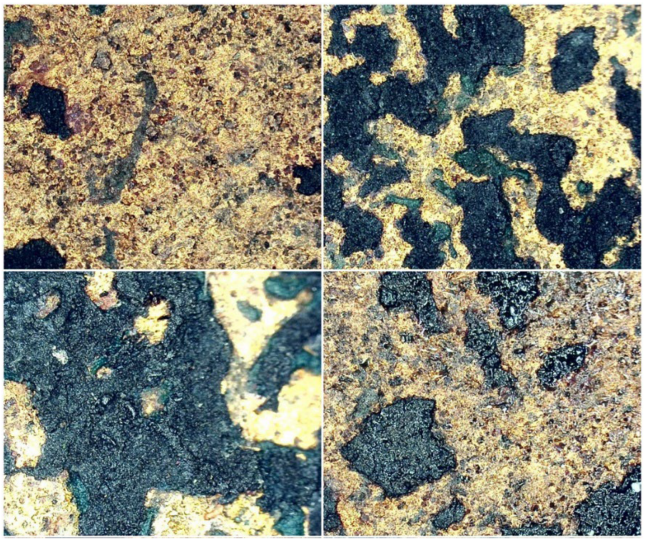

Figure 5. Corrosion at the tail of copper tube. **Source (s):** Authors' own work

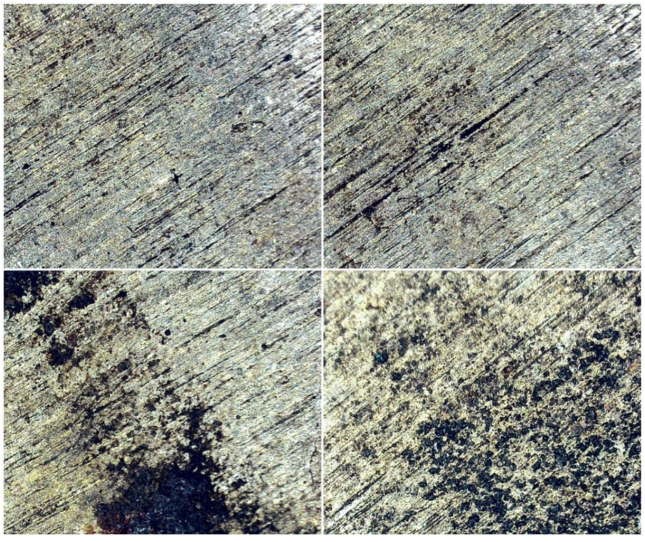

Figure 6. Corrosion at the head of copper tube. **Source (s):** Authors' own work

Yong, & Guo, 2015; Li, Han, Li, & Xin, 2017; Schlegel *et al.*, 2018; Yang, Hou, Zhang, & Li, 2017).

3.1.2 SEM and EDS characterisation.. Surface morphology observations were conducted on corrosion products at the tails of air conditioning copper tubes, with compositional analysis performed via EDS and line scanning. Results are presented in Table 2 and Figure 7. Numerous pitting corrosion sites were observed on the tube tails, exhibiting elevated proportions of Cu, C, and O elements. This primarily stems from the copper tubes' composition of Cu, Mo, and

Table 2. Elemental analysis of corroded outer surface of copper tube

Element	Mass fraction/% Tail	Head
C	32.28	30.01
O	13.57	16.84
Si	0.17	1.12
Na	0.60	1.1
Cu	50.04	47.87
P	0.80	1.50
K	0.95	1.72
Cl	0.27	0.50
Ca	0.19	0.17
Fe	0.47	0.52
Mo	0.50	0.44
Cr	0.17	0.20

Source(s): Authors' own work

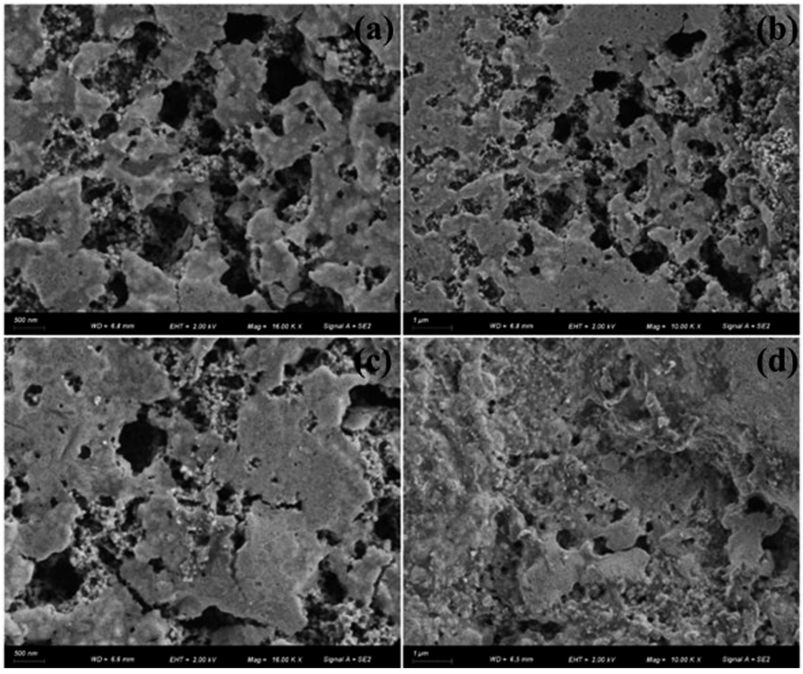

Figure 7. Copper Tube Corrosion (a), (b) Tail Corrosion Morphology (c), (d) Head Corrosion Morphology.
Source (s): Authors' own work

Cr, where elevated C and O content likely contributes to the formation of CuO and other non-metallic oxides (Bai, Liu, & Tu, 2014; Si, Xue, Sun, Liu, & He, 2019; Zhang, Wu, Shi, & Wang, 2025). Trace amounts of Si and Ca may have been introduced via atmospheric dust, while K and Na likely originated from alkaline substances used during cleaning. Corrosive Cl and P elements were also detected on the surface, constituting the primary causes of copper tube corrosion (Du *et al.*, 2025; Hemdan, Taha, Gabr, & Elkady, 2014; Liu, Qi, Wang, & Wan, 2025; Ma, Li, Xue, & Lai, 2018; Saengsod, Limmatvapirat, & Luangtana-Anan, 2012).

3.2 Effect of cleaning agents on air conditioning high-pressure shock-absorbing hoses

3.2.1 Continuous immersion and air exposure tests.. To investigate the effects of exterior cleaning agents on different materials of air conditioning compressor shock-absorbing hoses, the high-pressure shock-absorbing hose was dissected into 3 components: corrugated hose, pressure-bearing section, and copper tube. Continuous immersion and air exposure tests were conducted, and carry out continuous soaking (168 hours) and air exposure tests (soaking 1 hour, air exposure 23 hours; cycling 7 times), as illustrated in Figure 8. Microscopic images are shown in Figures 9 and 10.

The corrugated hose, pressure-bearing section, and copper tube were continuously immersed in 4 different cleaning agents. Solutions 1# and 5# turned blue upon immersion of

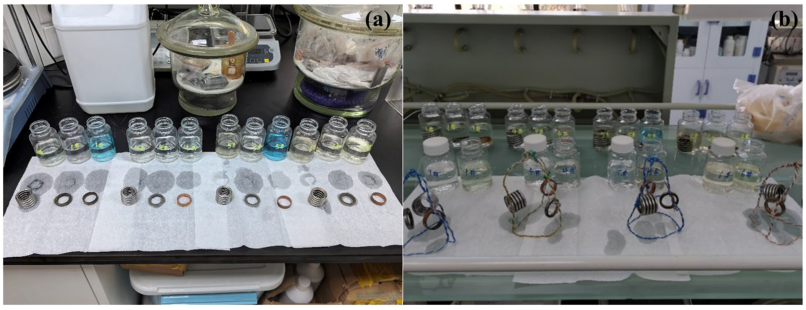

Figure 8. (a) Sample fully immersed (168h) (b) Sample exposed (168h). **Source (s):** Authors' own work

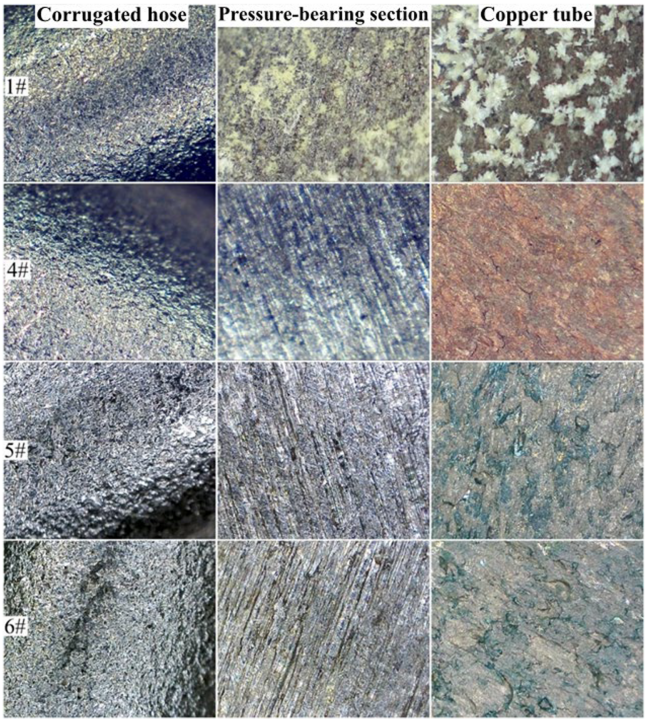

Figure 9. Microscopic image of the sample after 168 hours of immersion. **Source (s):** Authors' own work

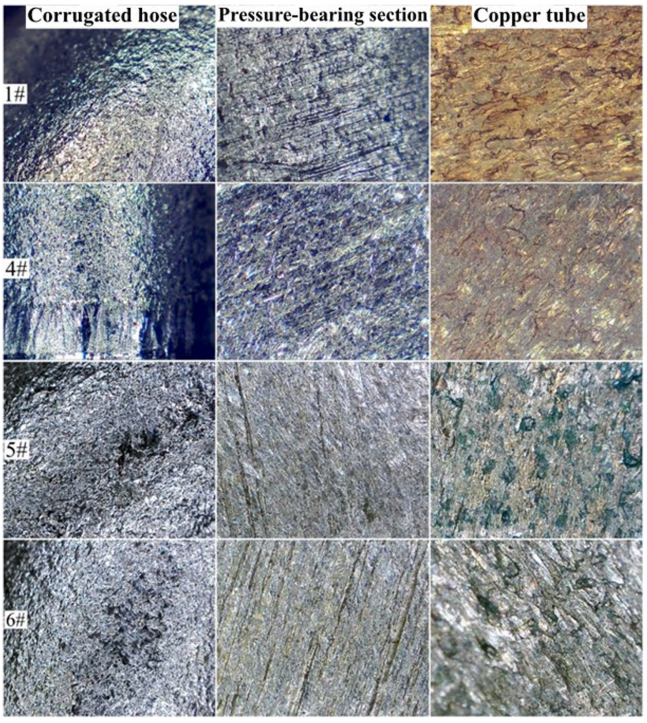

Figure 10. Microscopic image of the sample after 168 hours of air exposure. **Source (s):** Authors' own work

the copper tube, indicating the generation of Cu^{2+}. The copper tube reacted with the cleaning agents, forming dense pale yellow corrosion crystals on its surface. The quality changes of the copper tube were as follows: Cleaning agent 1# > Cleaning agent 6# > Cleaning agent 5# > Cleaning agent 4#. The compressed section exhibited more yellowish-brown corrosion products, with quality changes: Cleaning agent 1# > Cleaning agent 4# > Cleaning agent 5# > Cleaning agent 6#. The corrugated hose surface showed negligible changes, indicating that 304 stainless steel exhibits superior corrosion resistance compared to the other 2 materials. Consequently, it is evident that metal specimens undergo corrosion during prolonged immersion. The corrosion sequence of the metals is: Solution 1# > Solution 5# > Solution 4# > Solution 6#. Evidently, acidic and alkaline cleaning agents exert greater corrosive effects on metal specimens. Therefore, in subsequent component cleaning agent selection, priority should be given to neutral or weakly alkaline cleaning agents, avoiding acidic or strongly alkaline cleaning agent products. After cleaning, thorough water rinsing to neutrality (pH = 7) is mandatory, with residual residue inspection to prevent secondary corrosion.

Air exposure tests on metal specimens, corrugated hoses, pressure sections, and copper tubes indicate minimal mass change in metal specimens. Visual alterations to hoses, pressure sections, and copper tubes remain negligible, suggesting residual cleaning agent on metal surfaces. This is unlikely to adversely affect specimens in the short term.

It is also evident that the cleaning agent exerts a significantly greater impact on the pressure section (carbon steel) than on the corrugated hose (304 stainless steel) and copper tubing, as illustrated in Figure 11. Due to the higher chromium content in 304 stainless steel, the corrosion resistance of the stainless steel surface relies on the passivation film Cr_2O_3 formed by chromium. This film layer effectively isolates the corrosive medium from the base metal

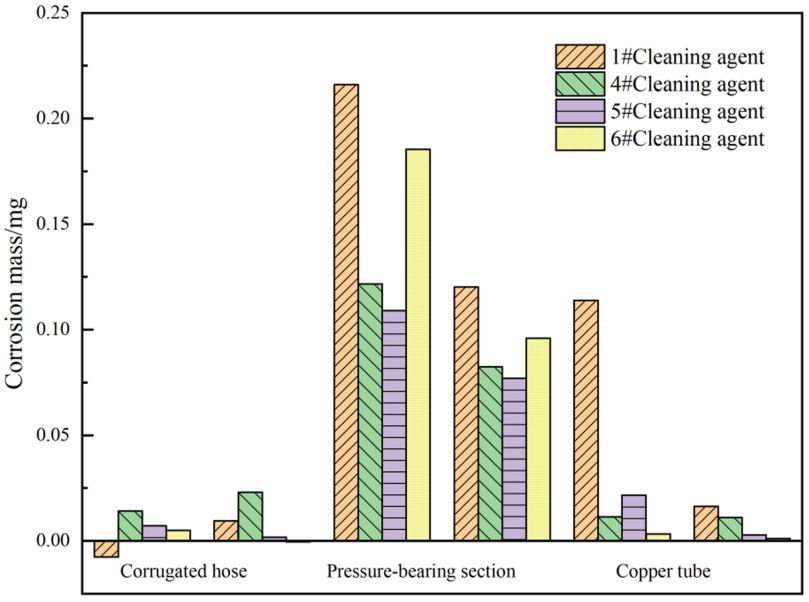

Figure 11. Changes in corrosion quality. **Source (s):** Authors' own work

through physical barrier action and electrochemical protection (Abdullah, El Nemr, El-Sakka, El-Hashash, & Soliman, 2021; El Nemr, Elhebshi, El-Deab, Ashour, & Ragab, 2022; Wen, Wu, Zhang, Zhang, & Xiao, 2021; Wang, Zhang, Ni, & Kong, 2026). Carbon steel, lacking corrosion-resistant elements, is susceptible to disruption by H^+ and OH^- ionsin acidic or alkaline cleaning agents. These ions destabilise the environment, causing Fe dissolution to form Fe^{2+}. The reduction process of H^+ produces highly reactive hydrogen gas, further promoting grain detachment and resulting in surface cracks of varying depths.

3.2.2 Microscopic morphology observation and elemental analysis.. After continuous immersion of the pressure section (carbon steel) and copper tube (TP2 deoxidised copper) in diluted solutions (1#, 4#, 5#, 6#, diluted to 20% concentration) for 168 hours, SEM examination of both specimens revealed: Acidic Cleaner 1# caused pronounced corrosion on both the pressure section and copper tube specimens. The pressure section specimen surface exhibited numerous yellowish-brown corrosion products that were loose, multi-layered, and prone to flaking. The outer surface of the copper tube specimen formed crystalline corrosion products. Cleaners 4#, 5#, and 6# had a lesser effect on the specimens, with the post-corrosion morphology being largely similar, as shown in Figure 12.

As indicated by the elemental analysis in Tables 3 and 4, the surface concentrations of S and Cl in samples immersed in Cleaning agent 1# were markedly higher than those in Cleaning agents 4#, 5#, and 6#. The H^+ ions in acidic cleaning agents constitute the primary driving force for corrosion (Galatis, Boyatzis, & Theodorakopoulos, 2012; Usman, Umoren, & Gasem, 2017; Zhang, Lin, & Yu, 2009; Zhao, 2024). Within an acidic environment, the porous oxide layer on carbon steel surfaces is rapidly dissolved by H^+ ions, exposing underlying Fe atoms directly to the acidic solution.

After applying the cleaning solution to the surface of the compressed section and copper tube, the specimens were exposed to air for 24 hours. This cycle was repeated 7 times. SEM observation of the 3 specimens revealed that the effects of the different cleaning agents were largely similar. Due to the relatively short contact time, the impact was minimal, as shown in Figure 13. Elemental analysis in Tables 5 and 6 indicates that the Fe content in the pressure-

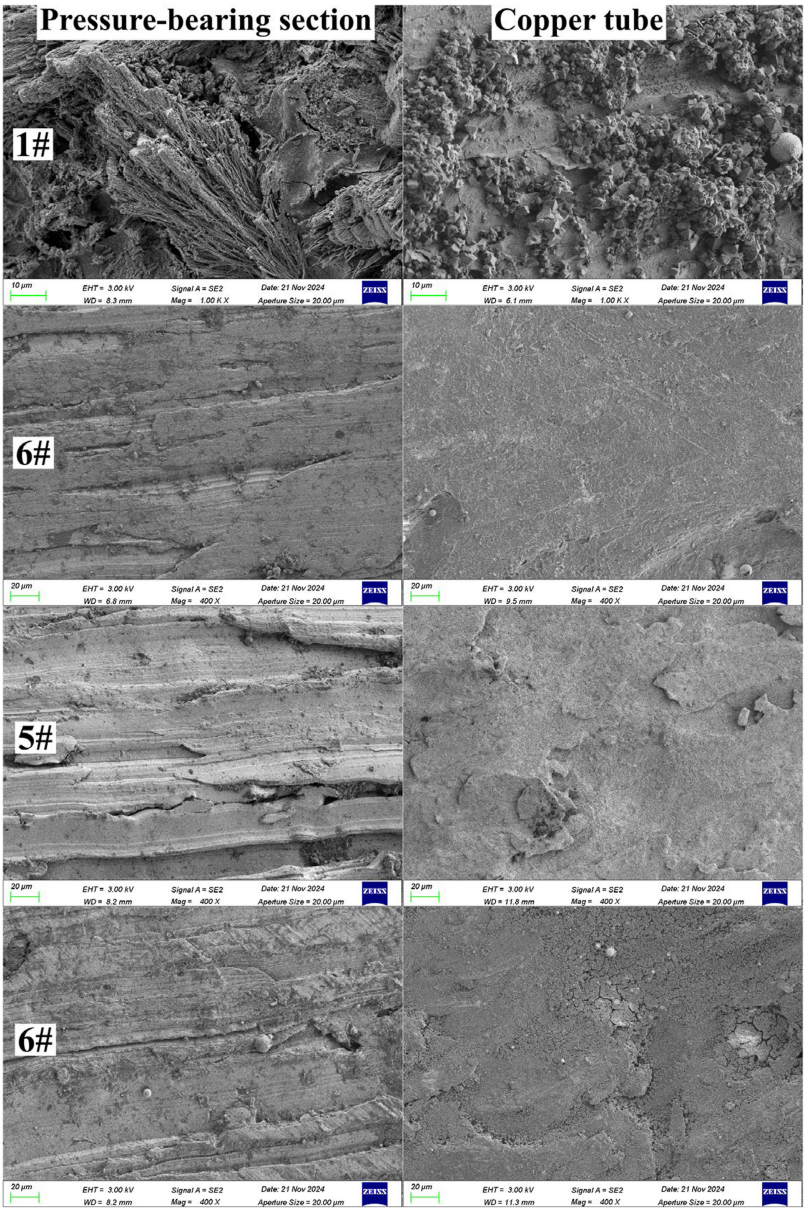

Figure 12. Electron microscopy images of the compressed section and copper tube after continuous immersion for 168 hours. **Source (s):** Authors' own work

bearing section sample and the Cu content in the copper tube sample immersed in Cleaning agent 1# were significantly lower than those treated with Cleaning agents 4#, 5#, and 6#. Cleaning agent 1# may have exerted a dissolving effect on the samples. For the pressure-bearing section specimens, this may stem from a minor reaction between H^+ ions in Cleaning agent 1# and Fe, causing partial Fe loss from the specimen surface in ionic form. Similarly, for

Table 3. Elemental analysis of compressed section after continuous immersion for 168 hours

Element (%)	1#	4#	5#	6#
C	35.85	12.38	13.53	20.87
O	19.9	5.34	6.34	5.59
Al	0.04	0.55	0.52	0.49
S	13.69	0.17	0.12	0.04
Cl	0.44	0.02	0.07	0.02
Fe	30.08	81.53	79.42	73
Cu	0	0	0	0

Source(s): Authors' own work

Table 4. Elemental analysis of copper tubes after continuous immersion for 168 hours

Element (%)	1#	4#	5#	6#
C	21.24	22.35	14.99	21.26
O	16.62	8.53	1.81	6.51
Al	0.4	0.07	0.01	0.15
S	12.5	0.34	0.03	0.11
Cl	0.41	0.2	0.01	0.07
Fe	0	0.38	0	1.19
Cu	48.83	68.12	83.15	70.72

Source(s): Authors' own work

the copper tube specimens, weak interactions between H^+ ions in Cleaning agent 1# and Cu resulted in minor Cu element depletion. The core chemical reaction is:

$$Fe + 2H^+ \rightarrow Fe^{2+} + H_2\uparrow$$

Acidic cleaning agents containing oxidising acid radicals (Cl^-, $SO_4{}^{2-}$) further accelerate the reaction by first oxidising Fe^{2+} to Fe^{3+}, forming insoluble $Fe_2(SO_4)_3$ precipitates that coat the surface as a corrosion product film. However, this film layer is loose and porous; it actually exacerbates localised corrosion due to acid solution retention beneath it (Du, Yi, & Shi, 2023; Kamal & Sethuraman, 2012). The core chemical reaction is:

$$Fe^{3+} + Cl_2 \rightarrow 2Fe^{2+} + 2Cl^-$$

$$2Fe^{2+} + SO_4^{2-} + 4H^+ \rightarrow 2Fe^{3+} + NO\uparrow + 2H_2O$$

Cu^{2+} generated during acidic corrosion may further combine with anions in solution (e.g. $SO_4{}^{2-}$, Cl^-) to form soluble salts (e.g. $CuSO_4$, $CuCl_2$). Consequently, scanning electron microscopy reveals crystals of soluble salts on the outer surface of copper specimens. Therefore, the core chemical reactions are:

$$2Cu + O_2 + 4H^+ \rightarrow 2Cu^{2+} + 2H_2O$$

3.2.3 Atomic force microscopy testing.. As shown in Figures 14 and 15, after continuous immersion for 168 hours, the maximum roughness of the compressed section ranged from −812.2 nm to −831.2 nm, with a minimum of −373.9 nm to −360.3 nm. The copper specimen

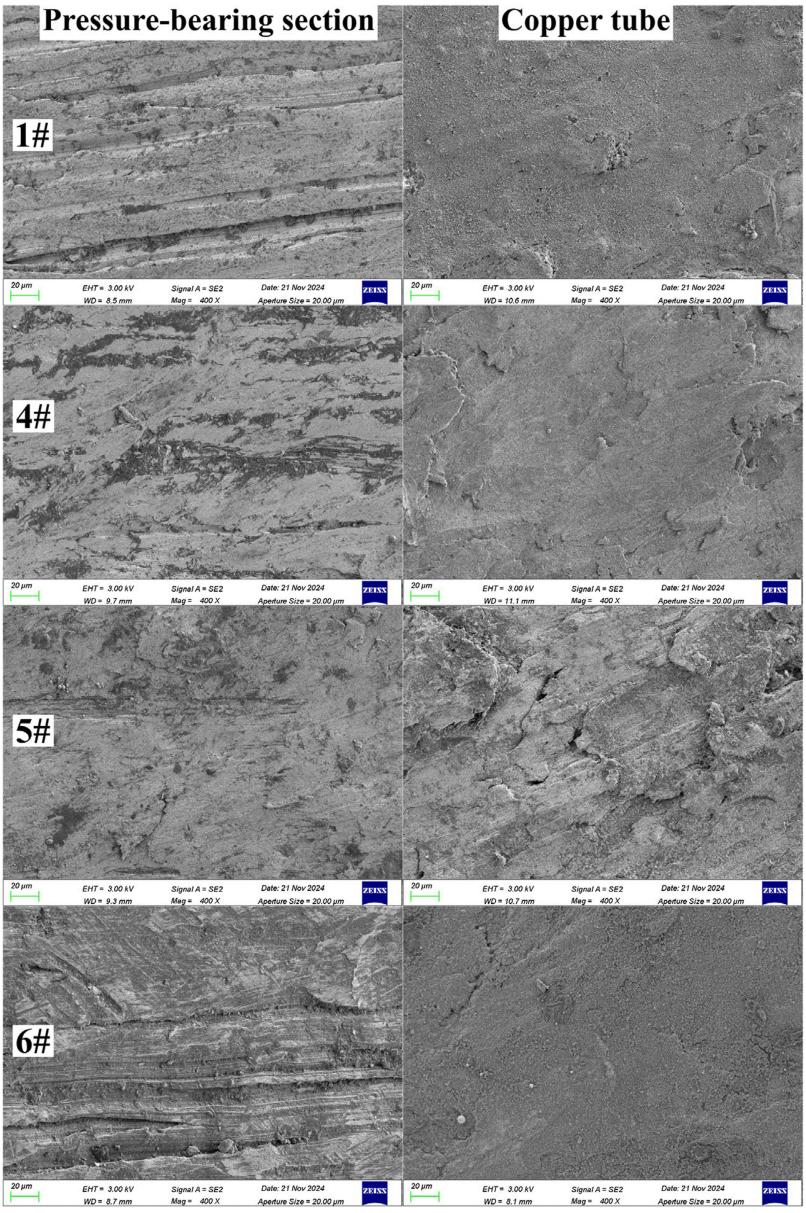

Figure 13. Electron microscopy images of the compressed section and copper tube after 168 hours of air exposure. **Source (s):** Authors' own work

exhibited a maximum roughness of −1.2 μm to −1.3 μm and a minimum of −427.9 nm to −396.6 nm. After 168 hours of air exposure, the maximum roughness of the compressed section ranged from −244.6 nm to −243.2 nm, with a minimum of −76.2 nm to −74.1 nm.

Table 5. Elemental analysis of compressed section after 168 hours of air exposure

Element (%)	1#	4#	5#	6#
C	22.79	19.74	17.27	11.91
O	14.68	6.82	6.35	10
Al	0.48	0.07	0.13	0.48
S	0.11	0.38	0.15	0.2
Cl	0.05	0.47	0.12	0.05
Fe	61.89	72.52	75.98	77.35
Cu	0	0	0	0

Source(s): Authors' own work

Table 6. Elemental analysis of copper tubes after 168 hours of air exposure

Element (%)	1#	4#	5#	6#
C	31.4	19.54	20.94	16.15
O	18.44	4.09	4.96	7.15
Al	0.09	0.09	0.07	0.1
S	6.96	0.4	0.13	0.18
Cl	0.09	0.14	0.11	0.15
Fe	0.97	0.2	0.67	1.67
Cu	42.04	75.54	73.11	74.61

Source(s): Authors' own work

The copper specimen exhibited a maximum roughness of −238.5 nm to −275.2 nm and a minimum of −124.3 nm to −115.0 nm. Both the corrosion depth and roughness of the compressed section and copper tube specimens after 168 hours of continuous immersion were greater than those after 168 hours of air exposure.

Atomic force microscopy results indicate that continuous immersion exhibits a higher corrosion rate. This is attributed to the liquid phase providing an ionic conduction medium, accelerating electrochemical corrosion processes. Dissolved oxygen (O_2) and Cl^- synergistically promote metal oxidation reactions. In contrast, atmospheric exposure corrosion proceeds more slowly, involving only surface-adsorbed water films in the reaction. The resulting oxidation products may form protective passivation layers, hence the slower corrosion rate.

4. Conclusions

Through analytical methods including SEM and atomic force microscopy, combined with corrosive element detection and cleaning agent immersion experiments, the causes of corrosion in metal components and the influence of cleaning agents were systematically investigated.

(1) Multiple corrosion patches and pitting were observed on the surface of the copper tube tail. The patches exhibited severe blackening, with elevated proportions of Cu, C, and O elements in the pitted areas. This is primarily because copper tubes are mainly composed of Cu, Mo, and Cr. The high C and O content likely resulted from the formation of corrosion products such as CuO and other non-metallic oxides. Additionally, corrosive Cl and P elements were detected on the surface, which are the primary causes of corrosion in copper tubes.

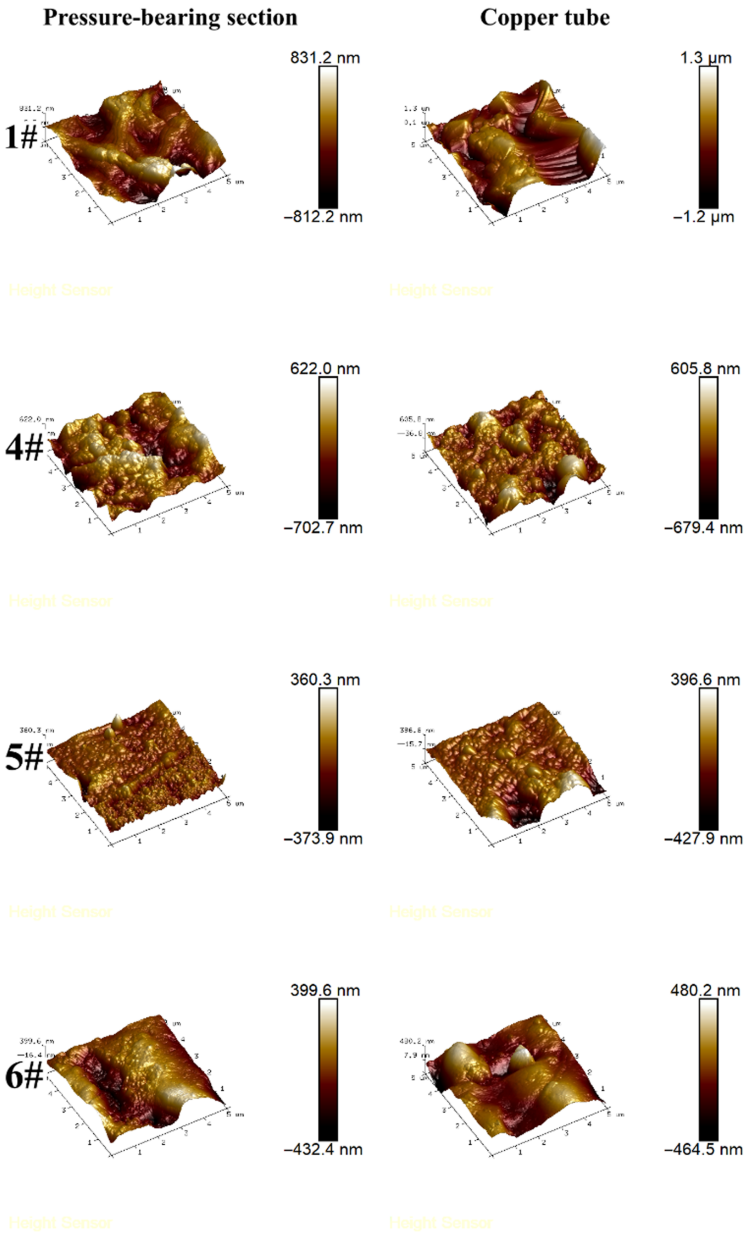

Figure 14. Atomic force micrographs of the compressed section and copper tube after 168 hours of continuous immersion. **Source (s):** Authors' own work

(2) Following continuous immersion testing, solutions 1# and 5# turned blue, indicating the generation of Cu^{2+}. The copper tubes reacted with the cleaning agent, forming dense, pale yellow corrosion crystals on their surfaces. The pressurised section (primarily carbon steel) exhibited significant yellowish-brown corrosion products.

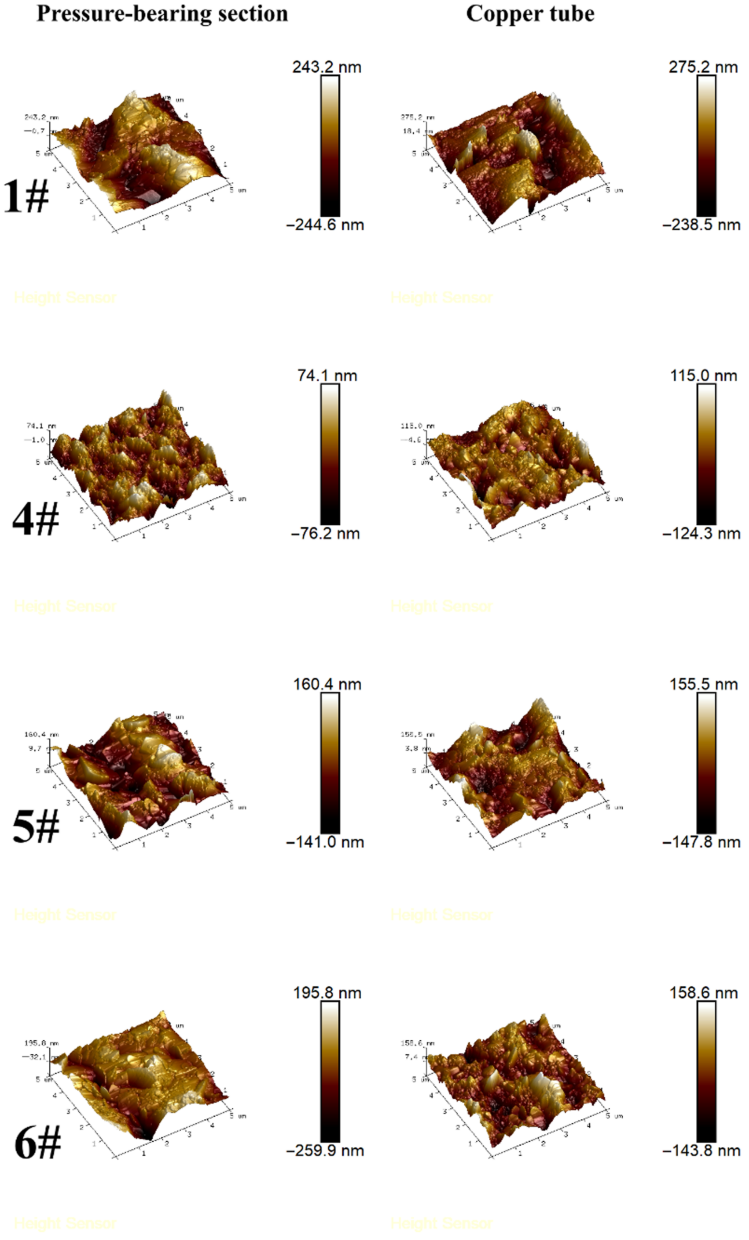

Figure 15. Atomic diagram of compressed section and copper tube after 168 hours of air exposure. **Source (s):** Authors' own work

The corrugated hose (primarily 304 stainless steel) showed no noticeable surface changes.

(3) Continuous immersion and air exposure tests demonstrate that corrosion under continuous immersion is significantly more severe than under air exposure. The liquid

phase environment provides an ionic conduction medium, accelerating the electrochemical corrosion process. Dissolved oxygen (O_2) and Cl^- synergistically promote the oxidation reaction of the metal.

(4) Acidic and alkaline cleaning agents exert significant corrosive effects on metal specimens. Consequently, neutral or weakly alkaline cleaning agents should be prioritised for subsequent component cleaning, avoiding acidic or strongly alkaline products. Post-cleaning, thorough water rinsing to neutrality (pH = 7) is mandatory, with residual residue inspection to prevent secondary corrosion.

References

Abd El-Maksoud, S. A. (2018). The effect of organic compounds on the electrochemical behaviour of steel in acidic media. A review. *International Journal of Electrochemical Science*, *3*(5), 528–555. doi: 10.1016/s1452-3981(23)15542-8.

Abdullah, R. S., El Nemr, A., El-Sakka, S. S., El-Hashash, M. A., & Soliman, M. H. (2021). Synthesis of phthalazinones with amino or hydrazide moiety as corrosion inhibitors of low carbon steel in 0.5 M H_2SO_4. *ChemistrySelect*, *6*(39), 10637–10647. doi: 10.1002/slct.202102513.

Bai, W., Yu, J., Yang, Y., Ye, Y., Guo, J., & Zhang, Y. (2013). Effect of CO_2 saturation on the corrosion behaviour of AZ31B magnesium alloy in Na_3PO_4 solutions. *International Journal of Electrochemical Science*, *8*(3), 3441–3453. doi: 10.1016/s1452-3981(23)14403-8.

Bai, H. P., Liu, J. R., & Tu, Y. Q. (2014). Analysis of surface corrosion defects on 05CuPCrNi weathering steel. *Surface Engineering and Remanufacturing*, *14*(5), 12–13.

Cheng, X. Y., Meng, F. J., Wang, N., Pang, X. B., & Duo, J. P. (2021). Failure analysis of CO2 air-conditioning pipelines for rail vehicles. *Railway Locomotive and Motor Car*, *4*(12), 17–21.

Deyab, M. A., Mohsen, Q., & Guo, L. (2022). Theoretical, chemical, and electrochemical studies of Equisetum arvense extract as an impactful inhibitor of steel corrosion in 2 M HCl electrolyte. *Scientific Reports*, *12*(1), 2255. doi: 10.1038/s41598-022-06215-6.

Du, W., Yi, Z. Y., & Shi, Z. P. (2023). Analysis on corrosion mechanism of C64 freight car material. *Advanced Materials for High Speed Railway*, *2*(5), 70–74.

Du, W., Tan, H. Y., Cui, D. S., Liang, J. Y., Yan, X., Ji, C. J., & Song, X. L. (2025). Effects of cleaning agents on aging behavior of rubber seals in EMU windshields. *Electroplating and Finishing*, *44*(6), 103–109.

Eddy, N. O., Ibok, U. J., Ebenso, E. E., El Nemr, A., & El Ashry, E. S. H. (2009). Quantum chemical study of the inhibition of the corrosion of mild steel in H_2SO_4 by some antibiotics. *Molecular Modeling*, *15*(9), 1085–1092. doi: 10.1007/s00894-009-0472-7.

El Nemr, A., El Said, G. F., Khaled, A., El Sikaily, A., Moneer, A. A., & Abd-El-Khalek, D. E. (2014a). Differences in the corrosion inhibition of water extracts of Cassia fistula L. pods and o-phenanthroline on steel in acidic solutions in the presence and absence of chloride ions. *Desalination and Water Treatment*, *52*(28/30), 5187–5198. doi: 10.1080/19443994.2013.807473.

El Nemr, A., Moneer, A. A., Khaled, A., El Sikaily, A., & El-Said, G. F. (2014b). Modeling of synergistic halide additives' effect on the corrosion of aluminum in basic solution containing dye. *Materials Chemistry and Physics*, *144*(1/2), 139–154. doi: 10.1016/j.matchemphys.2013.12.034.

El Nemr, A., Elhebshi, A., El-Deab, M. S., Ashour, I., & Ragab, S. (2022). Synergistic effect of Chitosan biguanidine hydrochloride salt as agreen inhibitor for stainless steel alloy corrosion in a 0.5 M H_2SO_4 solution. *Egyptian Journal of Chemistry*, *65*(2), 1–2.

Galatis, P., Boyatzis, S., & Theodorakopoulos, C. (2012). Removal of synthetic soiling mixture on mastic, shellac and Laropal K80 coatings using two hydrogels. *E-Preservation Science*, *9*, 72–83.

Hemdan, M. M., Taha, S. M., Gabr, A. M., & Elkady, M. Y. (2014). Synthesis of some new phthalazines and their evaluation as corrosion inhibitors of steel. *Journal of Chemical Research*, *38*(10), 617–621. doi: 10.3184/174751914x14116480062198.

Kamal, C., & Sethuraman, M. G. (2012). Caulerpin-A bis-indole alkaloid as a green inhibitor for the corrosion of mild steel in 1 M HCl solution from the marine alga Caulerpa racemosa. *Industrial and Engineering Chemistry Research*, *51*(31), 10399–10407. doi: 10.1021/ie3010379.

Li, M., Han, L. L., Li, H., & Xin, G. F. (2017). Study on corrosion and protection of special parts of petrochemical railway. *Chemical Engineering Design Communications*, *43*(6), 249.

Li, G., Bae, Y., Mishrra, A., Shi, B., & Giammar, D. E. (2020). Effect of aluminum on lead release to drinking water from scales of corrosion products. *Environmental Science and Technology, 54* (10), 6142–6151. doi: 10.1021/acs.est.0c00738.

Liu, L. R., Yong, X. Y., & Guo, F. Y. (2015). Research on the corrosion of metallic components of overhead contact system in typical atmospheric environment. *Journal of Railway Engineering Society*, *32*(3), 81–85.

Liu, X., G., Qi, S., Wang, Z., D., & Wan, D., T. (2025). Transverse vibration characteristics and influence of passenger car window glass in high-speed train passing through tunnel. *Railway Sciences*, *4*(4), 450–463. doi: 10.1108/rs-01-2025-0005.

Liu, W. H., Xu, C. K., Chen, H. H., & Zhang, Y. (2026). Electrochemical corrosion behavior of X80 pipeline steel in acidic and alkaline soil leachates. *International Journal of Pressure Vessels and Piping*, *220*, 105733. doi: 10.1016/j.ijpvp.2025.105733.

Ma, X., Li, J., Xue, T., & Lai, K. (2018). Study on stress and strain of pressure pipe with internal corrosion depression. *Journal of Plastic Engineering*, *25*(3), 267–273.

National Standardization Administration (2011). *GB/T 1690-2010 Rubber, vulcanized or thermoplastic-determination of the effect of liquids (Chinese Standard)*. Beijing: Standards Press of China.

Olasunkanmi, L. O., Obot, I. B., Kabanda, M. M., & Ebenso, E. E. (2015). Some quinoxalin-6-yl derivatives as corrosion inhibitors for mild steel in hydrochloric acid: Experimental and theoretical studies. *Journal of Physical Chemistry C*, *119*(28), 16004–16019. doi: 10.1021/acs.jpcc.5b03285.

Saengsod, S., Limmatvapirat, S., & Luangtana-Anan, M. (2012). A new approach for the preparation of bleached shellac for pharmaceutical application: Solid method. *Advanced Materials Research*, *506*, 250–253. doi: 10.4028/www.scientific.net/amr.506.250.

Schlegel, M. L., Necib, S., Daumas, S., Labat, M., Blanc, C., Foy, E., & Linard, Y. (2018). Corrosion at the carbon steel-clay borehole water interface under anoxic alkaline and fluctuating temperature conditions. *Corrosion Science*, *136*, 70–90. doi: 10.1016/j.corsci.2018.02.052.

Si, G. Q., Xue, Z. L., Sun, W. D., Liu, B. Y., & He, S. L. (2019). Analysis of the impact of internal and external corrosion on the remaining strength of concave pipelines. *Science and Technology and Innovation*, 23, 12–15.

Tan, B. Zhang, S., Qiang, Y., Feng, L., Liao, C., Xu, Y., & Chen, S. (2017). Investigation of the inhibition effect of Montelukast Sodium on the copper corrosion in 0.5 mol/L H_2SO_4. *Journal of Molecualr Liquids*, *248*, 902-910. doi: 10.1016/j.molliq.2017.10.111.

Thombare, N., Kumar, S., Kumari, U., Sakare, P., Yogi, R. K., Prasad, N., & Sharma, K. K. (2022). Shellac as a multifunctional biopolymer: A review on properties, applications and future potential. *International Journal of Biological Macromolecules*, *215*, 203–223. doi: 10.1016/j.ijbiomac.2022.06.090.

Usman, B. J., Umoren, S. A., & Gasem, Z. M. (2017). Inhibition of API 5L X60 steel corrosion in CO_2-saturated 3.5% NaCl solution by tannic acid and synergistic effect of KI additive. *Journal of Molecular Liquids*, *237*, 146–156. doi: 10.1016/j.molliq.2017.04.064.

Wang, F. Q., Zhang, K. W., Ni, X. R., & Kong, D. J. (2026). Post-treatment-controlled electrochemical behavior of laser cladded FeMnCoCrC high-entropy alloy coating. *Materials Letters*, *414*, 140527. doi: 10.1016/j.matlet.2026.140527.

Wen, J., Wu, Q. R., Zhang, L. Y., Zhang, S., & Xiao, Y. J. (2021). Research on the corrosion products of fracture failure high-strength bolt used in steel structure bridge. *Surface Technology*, *50*(5), 321–328, 347.

Yang, Y., Hou, H. X., Zhang, Z., & Li, L. (2017). Corrosion behavior of weathering bridge steel Q500qENH in simulated industrial atmospheric environment. *Corrosion and Protection*, *38*(4), 256–261.

Zhang, Y., Lin, J., & Yu, G. W. (2009). 304 stainless steel microbiological influenced corrosion characteristic research. *Surface Technology*, *38*(3), 44–45.

Zhang, Y., Wu, W., Shi, J. L., & Wang, Y. J. (2025). Ultimate load of high-grade steel pipes with corrosion depressions. *Science Technology and Engineering*, *25*(17), 7157–7164.

Zhao, L. M. (2024). Analysis of surface peeling defects on 022Cr18Ti stainless steel pickled plate. *Shandong Metallurgy*, *46*(4), 16–20.

Zheng, X., Gong, M., Li, Q., & Guo, L. (2018). Corrosion inhibition of mild steel in sulfuric acid solution by loquat (Eriobotrya japonica Lindl.) leaves extract. *Scientific Reports*, *8*(1), 9140. doi: 10.1038/s41598-018-27257-9.

Zhu, M. H., Yao, S. F., Xiang, X. M., Peng, J. F., Wang, J., Chen, X. J., . . . Wang, Z. Y. (2025). Failure analysis and whole life cycle management of rail transit equipment. *Materials for Rail Transportation System*, *4*(3), 1–14.

Further reading

China State Railway Group Co., Ltd (2025). *Q/CR468-2025 Cleaners for EMU exterior surface*. Beijing: China Railway Publishing House Co., Ltd.

National Standardization Administration (2014). *GB/T 30693-2014 Plastics-thin films and sheets-determination of contact angle*. (Chinese Standard). Beijing: Standards Press of China.

Corresponding author
Wei Du can be contacted at: Railwaydu@163.com